Interval Optimization Design of a Submersible Surface Ship Form Considering the Uncertainty of Surrogate Model

Yuejin Wan[1], Yuanhang Hou[1, 2#], Yeping Xiong[2], Zhenpeng Dong[1], Yuqi Zhang[1], Chao Gong[1]

1. Naval Architecture and Ocean Engineering College, Dalian Maritime University, Dalian 116026, China

2. Faculty of Engineering and Physical Sciences, University of Southampton, Boldrewood Innovation Campus, SO16 7QF Southampton, UK

Corresponding author: Yuanhang Hou

Email: houyuanhang@dlmu.edu.cn

Abstract

The integrated design of the ship form is a key issue in the design of submersible surface ship (SSS). In the simulation-based design (SBD) framework, lack of sample data leads to uncertainty in the surrogate model. In this paper, first, a hull cross-section shape modification technology, the self-fusion method, was used to change the ship form, and a fourth-order response surface model was introduced to establish surrogate model of hydrodynamic performance. Second, total resistance in the surface condition and one at a diving depth of 0.48 m were selected as the optimization targets. Third, an automated computing platform was developed to integrate the modules to improve computing efficiency and accuracy. Finally, to explore the adaptability of the ship form scheme, the interval optimization analysis method was introduced into uncertainty optimization. Among them, the interval variable was the surrogate model accuracy, and the targets were the minimum median and the minimum radius of the weighted resistance of cross-domain cases. A two-layer nested optimization system was chosen. Results show that resistance of the optimal SSS was reduced. The interval optimization results were compared with the deterministic optimization results, and the feasibility of hull shape interval optimization was verified.

Keywords： form optimization； submersible surface ship (SSS)； self-fusion method； interval optimization； uncertainly of surrogate model

Introduction

Unmanned ships have autonomous sailing capabilities and can perform dangerous tasks in the place of humans. Therefore, these ships have become a hot issue in the field of marine research [1]. In recent years, researchers have investigated the hydrodynamic, maneuvering, and self-propelled performance of various semi-submersible vehicles [2-3]. As a special semi-submersible vehicle, an SSS has semi-submersible concealment and high-speed surface sailing capabilities. It provides a new idea for the design of an underwater cross-domain vehicle [4]. Cross-domain SSSs mostly operate in surface cases. In bad weather or special missions, these ships can dive underwater. Therefore, it is necessary

to consider the optimal design of the ship form for cross-domain SSS cases.

Ship form optimization based on SBD technology includes a hull geometry reconstruction module, a hydrodynamic performance evaluation module, and an optimization algorithm module. Geometric reconstruction modules can be divided into two categories [5]. One is a surface-based modeling method. Non-uniform rational B-splines are used to represent surfaces. The method's main feature is that the hull surface is generated directly by the ship form coefficient. The surface can be smoothed by repeatedly adjusting the control points of the surface mesh [6-8]. If this method is applied to the hull geometry reconstruction module, the optimization variables are some or all of the grid point coordinates or the control point coordinates of the surface. This results in an unusually large number of optimization variables. Such proliferation of variables may result in inefficient and impractical optimization. Dimensionality reduction through sensitivity analysis (SA) is a feasible way to alleviate this problem. Liu et al. implemented a variance-based SA modeling method in a ship form optimization model and identified non-influencing variables for dimensionality reduction [9]. Another type of hull geometry reconstruction module is the parametric modeling technique. The specific method is to define the surface in the form of shape parameters [10-14]. These shape parameters are changed to alter the overall shape of the ship. The most significant advantage of parametric techniques is that small to moderate modifications can be made with only a few design variables. Therefore, this method facilitates rapid modification of the ship form. In the present study, the SSS had a high degree of integration, and the ship surface was excessively smooth. Therefore, a surface modification technology that parameterizes the ship's surface was adopted to realize three-dimensional surface deformation.

In recent years, SBD technology [15] developed by combining optimization technology with CFD technology has become more and more prominent in ship form design. Due to the limitation of computational cost, it is not feasible to completely execute the high-precision CFD solver at each step of the optimization iteration. The approximate model is used instead of the high-precision simulation model to solve the high response time and high computational cost brought by the high-precision CFD solver. The problem has become an effective means of ship form optimization design based on SBD technology. Commonly used approximate models include: response surface model (RSM), Kriging model and neural network model (NN) [16-19]. However, in the establishment of the approximate model, a large number of simulation calculation results are required as input samples, and the internal parameters of the algorithm are required to be strictly controlled. Therefore, there are inevitably many reasons for the poor accuracy of the approximate model, and the uncertainty of the cognitive response of the output results to the input variables will be caused by errors. Although this error or uncertainty has a small value in most cases, large deviation of the whole system can also be generated by continuous iterative computation. Therefore, it is of great theoretical and practical significance to consider the influence of uncertainty in the approximation model for ship form optimization design.

At present, there are many methods for solving uncertain optimization problems. According to the characteristics of uncertain parameters, they can be divided into three categories: stochastic programming, fuzzy programming and interval programming [20-22]. Among them, the stochastic programming method optimizes through random variables, and the probability density distribution of the random variables needs to be given. The parameters included in fuzzy programming are fuzzy numbers, and the membership function of the fuzzy numbers must be known in advance. However, it is difficult to obtain the above-mentioned probability density distribution and membership function in practical applications, so the application of these two methods in engineering is greatly limited [23]. The uncertainty optimization method based on interval programming takes the interval number as the

uncertainty parameter, and the upper and lower bounds or midpoint and radius of the interval number are required. This information is relatively easy to obtain in engineering applications, so interval uncertainty optimization has obvious advantages in engineering. At present, this method has been widely used in various engineering fields, such as profit maximization, wing design, automobile design, interior layout design, etc. [23], but the application in ship design is rarely reported.

In the research described in this paper, an automated optimization platform was built to optimize ship form of the SSS. Its purpose is to reduce the total resistance of SSS cross-domain sailing. First, six cross-sections of the ship were selected as the initial cross-sections, and they were expressed parametrically as design variables. To begin the optimization, a design space with upper and lower bounds on the design variables was constructed. These parameters were set around the SSS profile. The design space was then sampled using the Latin hypercubic method to generate the design matrix. A viscous flow solver was used to evaluate the total resistance of these designs. After the experimental design was completed, a fourth-order RSM [24] for the total resistance of the surface and underwater cases was constructed to reduce the time required for optimization. Then, three multi-objective optimization algorithms, non-dominated sorting genetic algorithm-II (NSGA-II), neighborhood cultivation genetic algorithm (NCGA), and adaptive mutation probability genetic algorithms (AMGA), were used for deterministic optimization. The overall workflow of the proposed optimization framework is shown in Figure 1. Finally, approximate models with different precisions were used as uncertain variables to participate in the calculation of uncertainty ship form optimization based on interval planning.

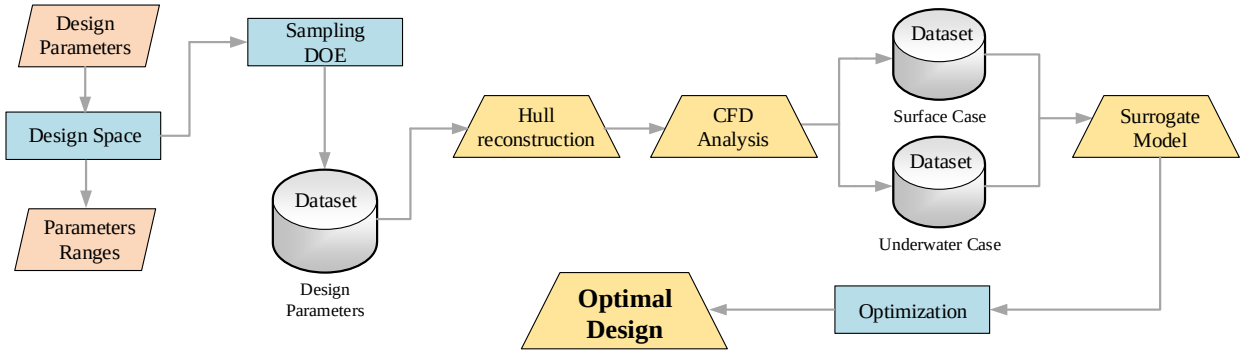

Fig. 1 Optimize overall workflow

1. Target ship and towing test

1.1 Target ship

Hirayama et al. proposed a design concept for a new type of SSS [25-26], as shown in Figure 2. The SSS has an irregularly shaped smooth main hull and a pair of main wings and ailerons located in the middle and the stern of the ship. In this study, only the sailing resistance of the main hull is considered, and the influence of appendages such as wings and rudders on the resistance performance is ignored. The cross-section of the SSS involved in the test is shown in Figure 3.

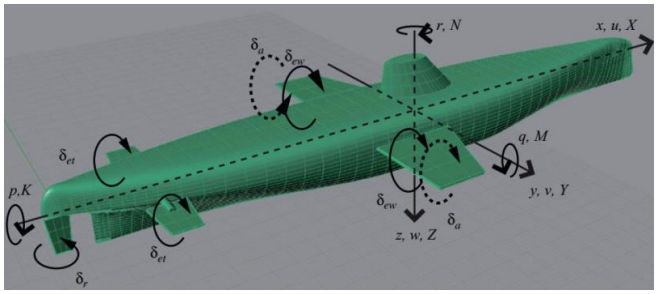

Fig. 2 Concept map of SSS

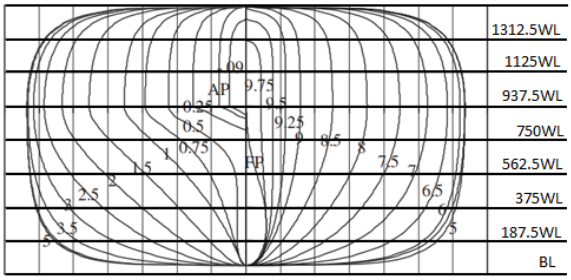

Fig. 3 Cross-section diagram of SSS

The main dimensions and related overall parameters of the test ship model are shown in Table 1.

Tab. 1 The value of the overall elements of the test ship model

Parameters	Unit	Value
Length overall (L_{oa})	m	1.6452
length between perpendiculars (L_{pp})	m	1.6000
Beam (B)	m	0.2322
Moulded depth（D）	m	0.1408
Draft（T）	m	0.0868
Free board（F）	m	0.0540
Wetted surface（A_w）	m^2	0.4451
Total surface （A_o）	m^2	0.8303

The scale of the ship model towing tank of Dalian University of Technology is 160.0 m × 7.0 m × 3.7 m (length × width × water depth). Trailer speeds range from 0.010 m/s to 8.000 m/s with a speed accuracy of 0.1%.

The ship model was processed and manufactured with numerical control machining equipment, and the processing accuracy of the ship model met the requirements of international towing tank conference (ITTC) standards. The SSS model is shown in Figure 4.

Fig. 4 Schematic diagram of the SSS model

The model was mounted on the bottom of the sword-shaped single point support, as shown in Figure 5, adjusted to 0 yaw and 0 elevation.

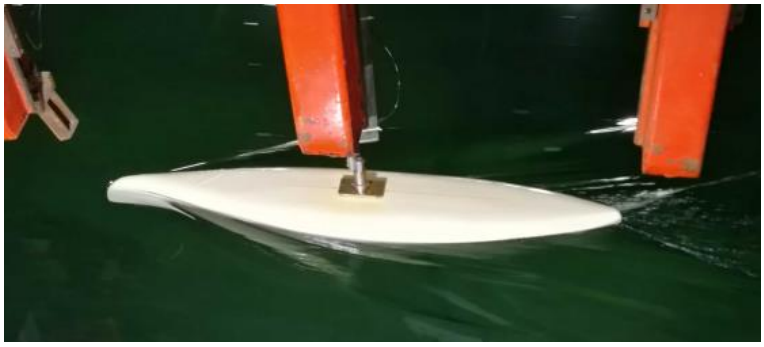

Fig. 5 Test setup diagram

1.2 Test plan and test results

Model resistance at different diving depths was tested. Calm water resistance at speeds of 0.4, 0.6, 0.8, 1.0, 1.1, 1.2, 1.3, 1.4, 1.5, 1.6, and 1.7 m/s was tested for each diving depth. Six working cases were tested, and the diving depth corresponding to case #0 to #5 was designed as the benchmark: 0, 0.054, 0.32, 0.48, 0.64, and 0.96 m, respectively. The definition of diving depth is shown in Figure 6.

After each group of towing experiments, the multi-speed test results of various cases were obtained. Since sensor itself is subjected to resistance due to water flow during measurement process, SSS's resistance of is equal to difference between resistance measured with sensor and resistance of the single sensor. The resistance of SSS by analyzing test data is listed in Table 2. The curve of above-mentioned V_m-R_{tm} measurement results is shown in Figure 7.

Tab. 2 Towing resistance results of SSS

V_m (m/s)	V_m (kn)	Fr	$Re(\times 10^6)$	R_{tm}/ (N)					
				#0	#1	#2	#3	#4	#5
0.4	0.78	0.101	0.528	0.29	0.27	0.39	0.37	0.28	0.33
0.6	1.17	0.152	0.793	0.54	0.54	0.72	0.71	0.62	0.70
0.8	1.56	0.202	1.057	0.84	0.99	1.22	1.25	1.15	1.22
1.0	1.94	0.253	1.321	1.22	1.42	1.95	1.89	1.79	1.87
1.1	2.14	0.278	1.453	1.47	1.68	2.22	2.28	2.23	2.23
1.2	2.33	0.303	1.585	1.81	2.37	2.67	2.69	2.62	2.68
1.3	2.52	0.328	1.717	2.10	2.79	3.21	3.15	3.07	3.17
1.4	2.72	0.353	1.850	2.72	4.30	3.86	3.71	3.54	3.60
1.5	2.92	0.379	1.982	3.90	7.02	4.72	4.31	4.13	4.06
1.6	3.11	0.404	2.114	5.70	10.54	5.83	5.00	4.71	4.66
1.7	3.30	0.430	2.246	7.61	14.39	6.96	5.82	5.37	5.23

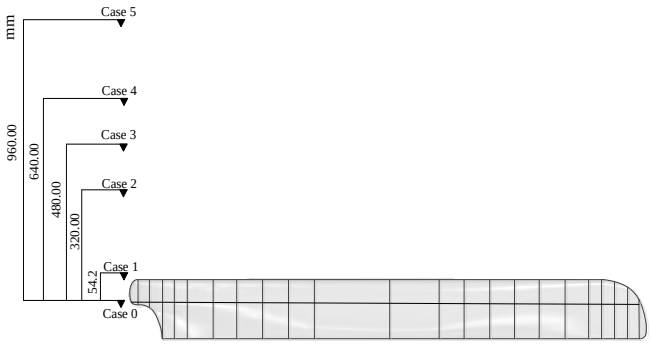

Fig. 6 Definition of diding depth for each working condition

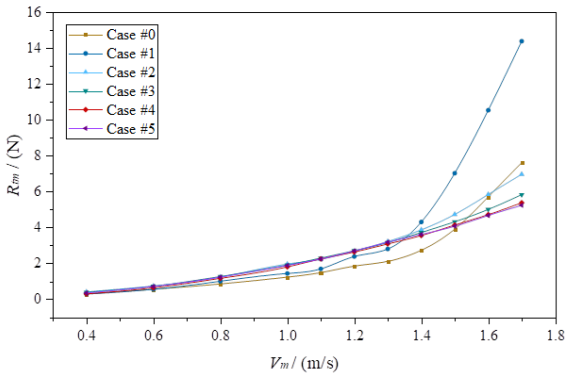

Fig. 7 The V_m-R_{tm} curve of the SSS

2. Numerical simulation of resistance

2.1 Numerical simulation setup

During the numerical simulation, the SSS moved in a straight line at a uniform speed with speed V. The flow about the ship can be observed from a righthanded moving system of orthogonal coordinates X $\equiv$ (X, Y, Z) attached to the ship (the X axis is chosen along the path of the ship and points toward the ship bow; the Y axis is parallel to the mean free surface and points toward the right side of the ship; and the Z axis is vertical and points upward, with the mean free surface taken as the plane Z = 0), as shown in Figure 8. The initial grid used for the SSS resistance calculation is illustrated in Figure 9. The grid numbers of surface and underwater cases are 1.36 million and 1.06 million, respectively. The y+ of first layer thickness is approximately 60 and the number of boundary layers is 5. The expansion ratio of the boundary layer is approximately 1.3. Simulations were performed using the standard solver STAR-CCM+. K-Epsilon model was used as the turbulence model [27]. The distance from bow one time the length of SSS as entrance, and the distance from stern two times length of SSS was defined as exit. The hull distance to upper boundary of calculation domain was one time length of ship, and lower boundary of the distance calculation domain was two times length of ship. To better present Kelvin waves in their entirety, shipboard distance from side boundary of computational domain was two times length of ship. The boundary conditions are set as shown in the Figure10.

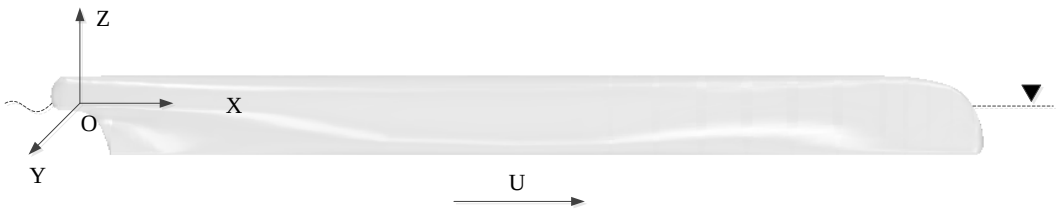

Fig. 8 Coordinate system definition diagram

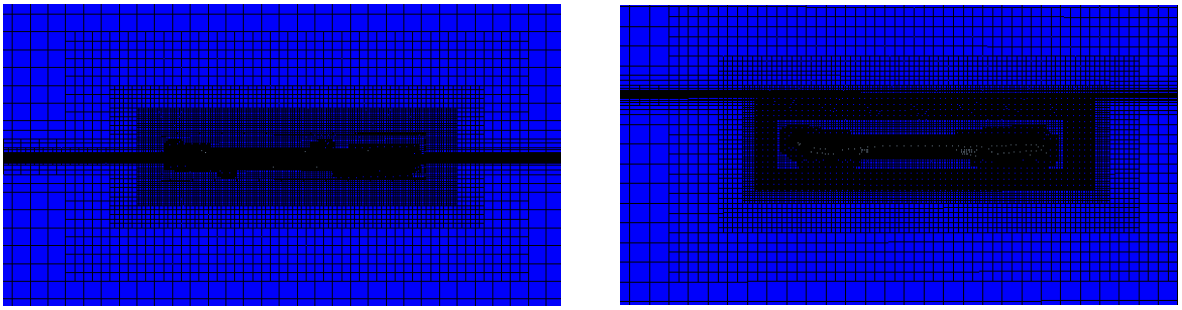

(a) Surface case (b) Underwater case

Fig. 9 Grid shape for SSS

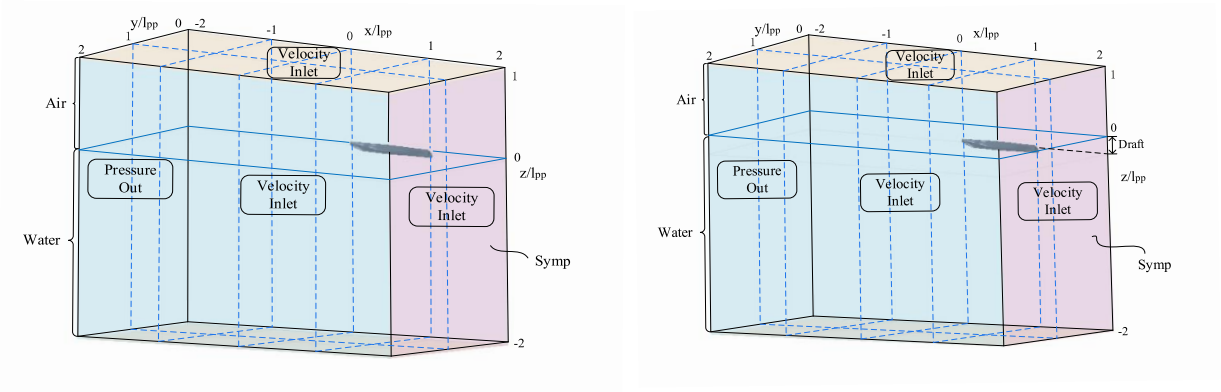

Fig. 10 Boundary condition display diagram for surface and underwater cases

2.2 Numerical calculation result comparison

To confirm the correctness of the mesh topology used in this study, a mesh independence analysis was performed for SSS of Case #0. Grid-independent validation was performed based on Richardson extrapolation, and three sets of different numbers of grids were generated. The time step was taken as 0.005 L_{pp}/V according to the recommendations specified by ITTC [27].

Tables 3-4 are the results of resistance deviation and independence analysis. In the table, C_t is the resistance coefficient of the SSS. R_G is the mesh convergence rate; U_G is uncertainty; D_0 is the corresponding test result; P_G is the accuracy order.

Tab. 3 Resistance results for V=1.2m/s

Parameter	Number of meshes /10^4	$C_t/10^{-3}$	Deviation /%
SSS test value	-	5.915	-
Fine mesh	283	5.841	1.25
Medium mesh	136	5.794	2.05
Coarse mesh	64	5.535	6.42

Tab. 4 Mesh verification analysis C_t

λ	R_G	P_G	(U_G/D_0)%
1	0.181	4.926	0.176

It can be seen from Table 3 that the resistance calculation results of the three sets of mesh at the model scale have high accuracy, and the deviation is within 7%. The mesh convergence rate R_G is less than 1, indicating that the mesh converges monotonically. The numerical uncertainty U_G is 0.176%D_0, indicating a high level of numerical simulation verification. In general, this mesh topology has good convergence and can be used for the study of the ship form optimization. The subsequent calculations are based on the coarse mesh, and the time cost can be reduced.

3. Self-fusion method

The self-fusion method [28] is a hull surface modification technology that parameterizes the 3D surface of the hull. First, a certain number of cross-sections at suitable locations are selected as initial cross-sections. Thus, the number of corresponding fusion factors (design variables) is determined. By

modifying the fusion factor, the deformation of the initial cross-section of the mother ship is realized. Then, the interpolation factor of the corresponding cross-section is obtained by using the feature point data of the profile line of the mother ship cross-section. Finally, other cross-sections are obtained according to the initial cross-section of the new ship and the interpolation factor to obtain the new ship. The flowchart of the self-fusion method is shown in Figure 11.

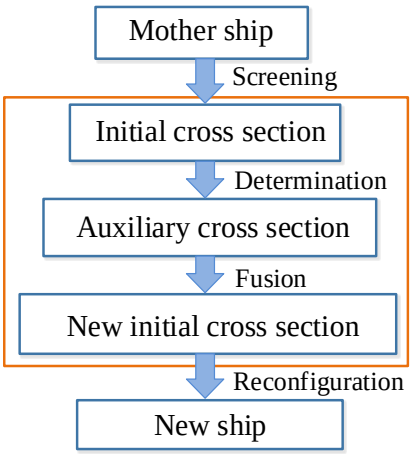

Fig. 11 Flow chart of self-fusion method

3.1 Selection of the initial cross-section

The shape of the cross-section contour line at the parallel mid-body of the ship is basically the same. However, the curvature of the contour line at the bow and stern changes considerably. Therefore, invalid cross-sections will be generated due to the uniform extraction method. This results in a waste of resources for subsequent optimization calculations. Based on the analysis above of the longitudinal change in the ship, the method of expanding from the midship to the fore and aft ends was adopted. Section 11 was selected as the reference, and sections 17, 19, and 21 along the x-axis forward direction were selected as the initial cross-sections. Sections 4 and 2 along the x-axis stern direction were selected as the initial cross-sections. A schematic diagram of the location of the initial cross-section is shown in Figure 12.

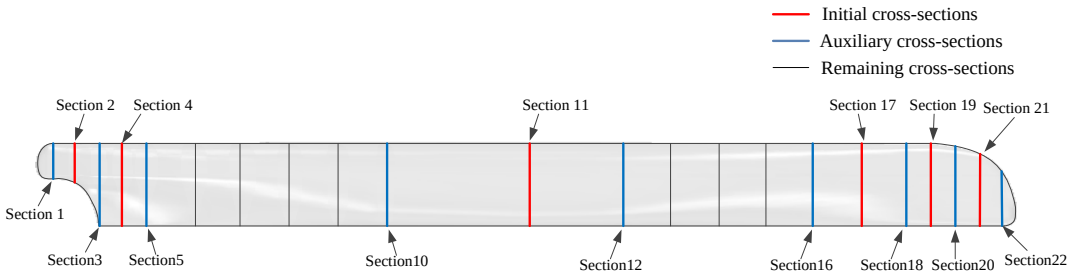

Fig. 12 Schematic diagram of initial cross-section position

3.2 Auxiliary cross-section selection and intercept feature point coordinates

After the position of the initial cross-section has been determined, the auxiliary cross-section must be selected. The initial cross-section requires the selection of two adjacent auxiliary cross-sections. A schematic diagram of auxiliary cross-section selection is shown in Figure 13. In the figure, b is the initial cross-section, and a and c are the auxiliary cross-sections. Based on the selection method for the auxiliary cross-section and the position of the initial cross-section introduced above, sections 22 and 20 are determined to be the auxiliary cross-section of section 21. Sections 20 and 18 are designated as auxiliary cross-sections of section 19. Sections 18 and 16 are designated as auxiliary cross-sections of

section 17. Sections 12 and 10 are designated as auxiliary cross-sections of section 11. Sections 5 and 3 are defined as auxiliary cross-sections of section 4. Sections 3 and 1 are designated as auxiliary cross-sections of section 2. This is used to fuse the initial cross-section of the new ship.

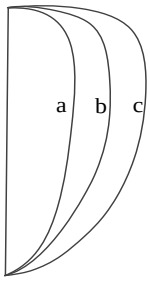

Fig. 13 Auxiliary cross-section selection diagram

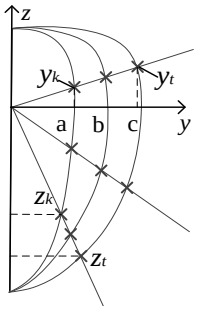

Fig. 14 Schematic diagram of feature point interception method

To integrate the initial cross-section of the new ship, the coordinates of the feature points of the target ship contour line must be extracted. The feature point interception method is shown in Figure 14. The interception method of the intersection of the ray with the design waterline as the origin and the contour line is adopted. The y- and z-coordinates of the intersection point on the same longitudinal ray are not equal. Then, the coordinates of the initial cross-section feature points of the new ship are found as follows:

$$\begin{aligned} y' &= w * y_k + (1-w) * y_t \\ z' &= w * z_k + (1-w) * z_t \end{aligned} \tag{1}$$

where y' and z' are the y- and z-coordinates of the feature point of the initial cross-section contour line of the new ship. w is the fusion factor. As shown in Figure 14, y_k and y_t are the y-coordinates of the feature points of the contour lines of the auxiliary cross-sections a and c, respectively, and z_k and z_t are the z-coordinates of the feature points of the contour lines of the auxiliary cross-sections a and c.

3.3 Rebuilding of the new ship

A total of six cross-sections were screened for the target ship above, corresponding to six fusion factors w_1 to w_6. Combined with formula 1, the auxiliary cross-section of the target ship was fused to obtain the initial cross-section of the new ship. The initial value of the fusion factor is shown in Table 5.

Tab. 5 Initial value of fusion factors

Fusion factor	Variable interval	Initial value
w_1	[0,1]	0.546
w_2	[0,1]	0.642
w_3	[0,1]	0.813
w_4	[0,1]	0.235
w_5	[0,1]	0.763
w_6	[0,1]	0.663

After the initial cross-section of the new ship is fused, the remaining cross-sections must be obtained by interpolation. First, the y- and z-coordinates of each cross-section feature point are obtained, and then the distance between the feature points corresponding to the contour lines between two adjacent profiles is calculated. The calculation formula is as follows:

$$d_j = \sqrt{\left(y_{ij} - y_{i+1,j}\right)^2 + \left(z_{ij} - z_{i+1,j}\right)^2} \tag{2}$$

In the formula, d is the distance between the corresponding feature points of two adjacent contour lines, y is the y-coordinate of the feature point, z is the z-coordinate of the feature point, i is the number of the i-th cross-section; j is the number of the j-th feature point on the contour line.

Second, the average value of the distance between the corresponding feature points of two adjacent contour lines is required. Assuming that each contour line takes m points, this paper takes 22 points for each contour line, as follows:

$$D_i = \frac{\sum_{j=1}^{m} d_j}{m} \tag{3}$$

In the formula, D is the average value of the distance between the corresponding feature points of two adjacent contour lines, m is the number of feature points of each contour line, d is the distance between the corresponding feature points of two adjacent contour lines, and j is the feature point number of the contour line.

Next, the interpolation factor for each section needs to be calculated. Take the calculation of the interpolation factor of section 11 to section 17 as an example. That is, the y- and z-coordinates of sections 12, 13, 14, 15, and 16 are obtained by interpolating (Section 11 and Section 17 have been obtained through the above calculation). The calculation formula is as follows:

$$\begin{cases} W_{12} = \dfrac{D_{12}}{D_{12} + D_{13} + D_{14} + D_{15} + D_{16} + D_{17}} \\ W_{13} = \dfrac{D_{12} + D_{13}}{D_{12} + D_{13} + D_{14} + D_{15} + D_{16} + D_{17}} \\ W_{14} = \dfrac{D_{12} + D_{13} + D_{14}}{D_{12} + D_{13} + D_{14} + D_{15} + D_{16} + D_{17}} \\ W_{15} = \dfrac{D_{12} + D_{13} + D_{14} + D_{15}}{D_{12} + D_{13} + D_{14} + D_{15} + D_{16} + D_{17}} \\ W_{16} = \dfrac{D_{12} + D_{13} + D_{14} + D_{15} + D_{16}}{D_{12} + D_{13} + D_{14} + D_{15} + D_{16} + D_{17}} \end{cases} \tag{4}$$

In the formula, W_{12} is the interpolation factor of section 12. Similarly, W_{13}, W_{14}, W_{15}, and W_{16} can be obtained. D_{12} is the average distance between the corresponding feature points of sections 12 and 13. Similarly, D_{13}, D_{14}, D_{15}, and D_{16} can be obtained.

After the interpolation factor is obtained, the y and z coordinates of the sections 12-16 can be obtained through the section 11 and the section 17.The formula is as follows:

$$\begin{cases} y_{12,j} = W_{12} * y_{17,j} + \left(1 - W_{12}\right) * y_{11,j} \\ z_{12,j} = W_{12} * z_{17,j} + \left(1 - W_{12}\right) * z_{11,j} \end{cases} \tag{5}$$

In the formula, $y_{12,j}$ is the y-coordinate of the j-th feature point on the contour line of section 12.

Similarly, $y_{13,j}$, $y_{14,j}$, $y_{15,j}$, and $y_{16,j}$ can be obtained. $z_{12,j}$ is the z-coordinate of the j-th feature point on the contour line of section 12. Similarly, $z_{13,j}$, $z_{14,j}$, $z_{15,j}$, and $z_{16,j}$ can be obtained.

Therefore, the y- and z-coordinates of the feature point of section 12 are calculated. In the same way, the y- and z-coordinates of the feature points of sections 13, 14, 15, and 16 can be obtained.

Taking the above calculation as an example, the y-coordinate and z-coordinate of the feature points in sections 2 to 4, 4 to 11, 17 to 19, and 19 to 21 can be calculated in the same way. The x-coordinates of the feature points can be calculated from the length of the ship. Thus, all coordinates of the feature points of each section of the new ship were obtained. Figure 15 is a three-dimensional surface comparison diagram of new ship and initial ship.

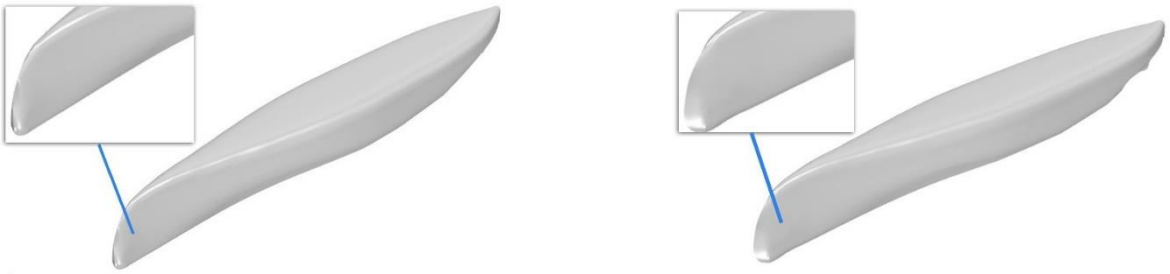

(a) Initial ship (b) New ship

Fig. 15 SSS 3D surface comparison diagram

4. Surrogate model building

To speed up the optimization process, fourth-order resistance response surface models of the surface case (Case A) and the underwater case with a diding depth of 0.48 m (Case B) were established. In the process of ship form optimization, four steps are required to establish a surrogate model. The specific steps are shown in Figure 16.

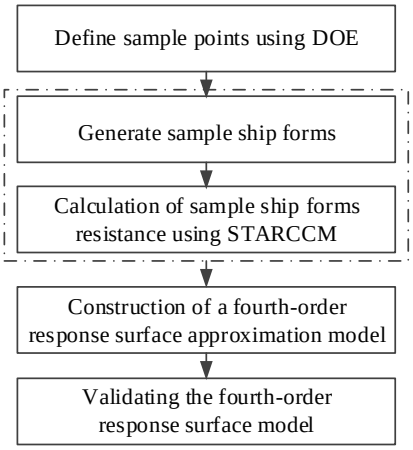

Fig. 16 Surrogate model establishment flowchart

Design of experiments (DOE) is a strategy for selecting sample points in the design space. Its purpose is to maximize the amount of information obtained. In this study, the Latin Hypercube (LHS) technique [29] was used to allocate 60 sets of sample points in the design space. Once the sample points were generated in the design space, a new ship could be generated using the self-fusion method. Then, 60 groups of new ships were calculated using simulation software to evaluate the total resistance of these new ships in Case A and Case B. The optimization problem of ship form is relatively complex. Therefore, a fourth-order response surface mathematical model is constructed in this paper. Six design

variables determine the reconfiguration of the hull geometry. According to formula 6, there must be at least 40 sample points. Therefore, 60 sets of sample points were obtained through LHS technology to ensure that the mathematical model had credibility

$$\begin{cases} P_1 = M + 1 \\ P_2 = (M+1)(M+2)/(n-2) + M \end{cases} \tag{6}$$

In the formula, M is the number of design variables, n is the order of the response surface model, P_1 is the number of sample points required for the first-order response surface model, and P_2 is the number of sample points required for the second- to fourth-order response surface model.

In this paper, 60 groups of experimental design sample points were obtained. Each group of sample points corresponded to two sets of responses of Case A and Case B; thus, 120 sets of responses were obtained. Then, the response and sample points were used to construct a polynomial response model. In this process, 120 groups of samples were meshed and numerically calculated using simulation software. If performed manually, the process is tedious and error-prone. Therefore, Isight (a multi-parameter and multi-disciplinary optimization tool platform) was used to build an automated platform for simulation calculations to construct a surrogate model. The automation platform is shown in Figure 17.

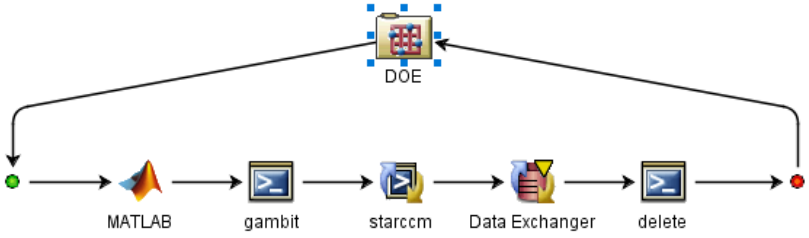

Fig. 17 Automated Computing Platform

The workflow of the platform is as follows: First, the Latin hypercube sample points are generated by the DOE component and passed to the MATLAB component. Second, the new hull feature points are generated by MATLAB, and the feature points are exported as a .dat file. Third, the .dat file is used by the Gambit component to generate and export the hull model in .stp file. Then, meshing and numerical calculation are performed in Star-ccm+, and the numerical results are exported to a .csv file. Finally, the average value of the numerical results is obtained by the Data exchanger component and passed to the DOE component. To ensure that the experimental design process is carried out normally, the delete component is used to delete some repetitive files generated during each cycle. After the experimental design is completed, a response surface model is constructed using the calculation results.

After 120 cycles of the optimized platform, responses corresponding to the 120 groups of sample points were obtained. Some calculation results are shown in Table 6.

Tab. 6 Part of the calculation results of the automation platform

Variables / Serial number		w_1	w_2	w_3	w_4	w_5	w_6	R_tN)
Case A	1	0.017	0.169	0.119	0.949	0.542	0.017	1.9882
	2	0.356	0.085	0.763	0.966	0.153	0.881	1.7928

	3	0.525	0.593	0.576	0.458	0.61	0.763	1.8946
	4	0.695	0.339	0.898	0.051	0.864	0.153	1.7366
	5	0.831	0.983	0.458	0.186	0.22	0.949	1.8684
Case B	1	0.068	0.593	0.017	1	0.322	0.949	2.6040
	2	0.356	0.254	0.424	0.102	0.356	0.831	2.5494
	3	0.61	0.898	0.288	0.322	0.763	0.508	2.5636
	4	0.322	0.576	0.542	0.102	0.356	0.576	2.5394
	5	0.915	0.237	0.339	0.644	0.254	0.169	2.5610

Based on the numerical calculation results, the Case A and Case B response surface models were constructed. Y_1 represents the total resistance of Case A, and Y_2 represents the total resistance of Case B. The complex correlation coefficient R^2 was used to verify the reliability of the model. The closer the value of R^2 is to 1, the higher the reliability of the mathematical model. Generally, when the R^2 value is greater than 0.9, the mathematical model is considered a substitute for the simulation program. As shown in Figure 18, the R^2 of the Case A and Case B of response surface models is 0.966 and 0.946, respectively; thus, they can replace the simulation program.

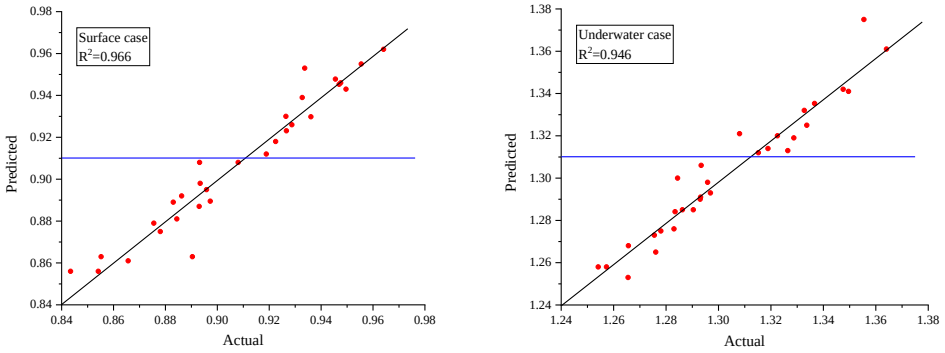

Fig. 18 Surrogate model Error Analysis Plot

The proportion of fusion factor weights represents the contribution of each factor to the response. Figure 19 shows that the weight of w_4 on the resistance of the SSS is the largest, and the weight of w_5 on the resistance is second only to that of w_4. For Case A, w_1 and w_2 have the least influence on the resistance; however, for Case B, w_2 and w_3 have the least influence on the resistance. The fusion factor w_1 controls the fusion of section 21, w_2 controls the fusion of section 19, w_3 controls section 17, and w_4, w_5, and w_6 control sections 11, 4, and 2, respectively. For the research objective of this paper, the shape of the midship has the greatest influence on the resistance of the SSS, the shape of the stern has the second greatest influence on the resistance, and the shape of the bow has the least influence on the resistance. In the figure, blue indicates a positive correlation, and red indicates a negative correlation.

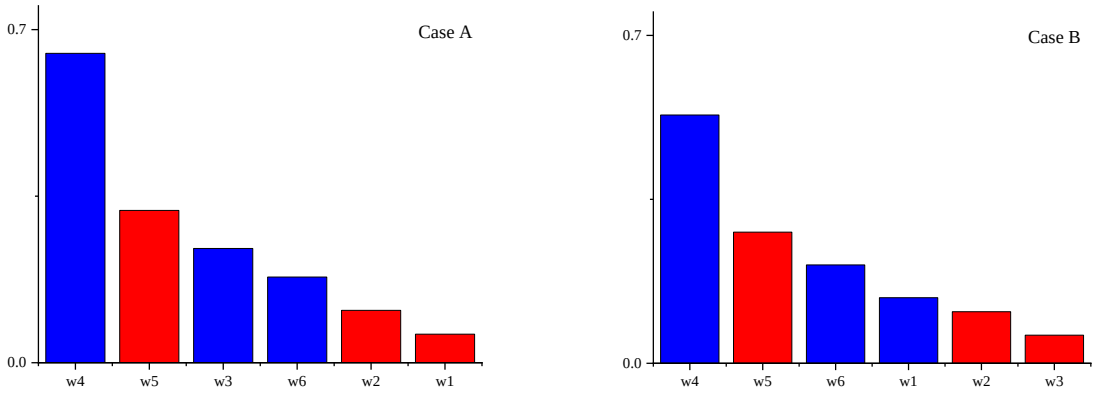

Fig. 19 Fusion factor contribution

5. Deterministic optimization

To obtain the ship with the least resistance in the cross-domain sailing state, the mathematical model of the surface and underwater cases obtained above was used instead of the simulation program for global optimization. The ships with the smallest total resistance corresponding to the fusion factors w_1 to w_6 within the specified range were obtained by searching. The optimization platform was built, and the workflow of the platform was as follows: The mathematical expression of the polynomial response surface model constructed above was entered into the Calculator component (a component in Isight software). Parameters in the Calculator component were mapped to the Optimization component (a component in Isight software).

NCGA, NSGA-II, AMGA are three kinds of multi-objective genetic algorithms. The advantage of NSGA-II is that the exploration performance is good. In the non-dominated ranking, because the individuals close to the Pareto frontier are selected, the Pareto advance ability is enhanced. Each objective is regarded as equally important by the NCGA, and its computational convergence process can be accelerated. An archive is established by the AMGA algorithm outside the evolution process to save the non-dominated individuals and the corresponding multi-objective function values in the evolution process. The saved feasible non-dominated designs constitute the optimal Pareto frontier. The three algorithms were selected to optimize the response surface model globally. Then, the accuracy and efficiency of the algorithms were compared. The description of the optimization problem is shown in Tables 7 and 8.

Tab. 7 Cross-domain optimization problem description

Two-objective optimization: ● Minimum R_t in surface case ● Minimum R_t in underwater case
Design variables: w_1, w_2, w_3, w_4, w_5, w_6
Constraints: ◆$0 \leq w_1 \leq 1$ ◆$0 \leq w_2 \leq 1$ ◆$0 \leq w_3 \leq 1$ ◆$0 \leq w_4 \leq 1$ ◆$0 \leq w_5 \leq 1$

◆$0 \leq w_6 \leq 1$ ● Keep ▽constant
Constants: ● Traveling speed：V=1.2(m/s)

Tab. 8 Optimization algorithm settings

● NSGA-Ⅱ:	● NCGA:	● AMGA:
Population size:12	Population size:12	Initial size:40
Number of geneation:30	Number of geneation:30	Population size:40
Crossover probability:0.9	Crossover type:1	Number of function evaluation:500
Crossover distribution index:10	Crossover rate:1	Crossover probability:0.9
Mutation distribution index:20	Mutation rate:0.01	Mutation probability:0.5

In the process of optimization, the selection of constraints was difficult. The entire hull form optimization was formulated to minimize total resistance under design conditions while satisfying the geometric constraints. The new hull form was subject to the following constraints:

The constraint is the ship displacement volume is a constant.

To obtain a reliable and flexible hull, technological constraints had to be considered as well. These constraints provided the upper and lower bounds of the design variables.

The results for the three algorithms are shown in Table 9. The schematic diagrams of the Pareto solutions of the three algorithms are shown in Figure 20. The AMGA is inefficient for this problem; the Pareto solution requires 22.7 evaluations, and the Pareto solution is not uniform and continuous enough. Although the NCGA is relatively highly efficient, the Pareto solution requires 9.4 evaluations, but the Pareto solution is not continuous enough. The NSGA-II is highly efficient, the Pareto solution requires 7.4 evaluations, and the Pareto solution has good continuity and uniformity. Therefore, the results for the NSGA-II were selected as the optimization results and were used for the subsequent comparison of the uncertainty interval optimization.

Tab. 9 Comparison of optimization algorithm results

Algorithm	Number of Pareto solutions	Total evaluations	The number of evaluations required for a Pareto solution	Pareto solution	
				Y_1	Y_2
AMGA	23	501	22.7	1.786	2.550
NCGA	32	301	9.4	1.750	2.582
NSGA-Ⅱ	49	361	7.4	1.766	2.556

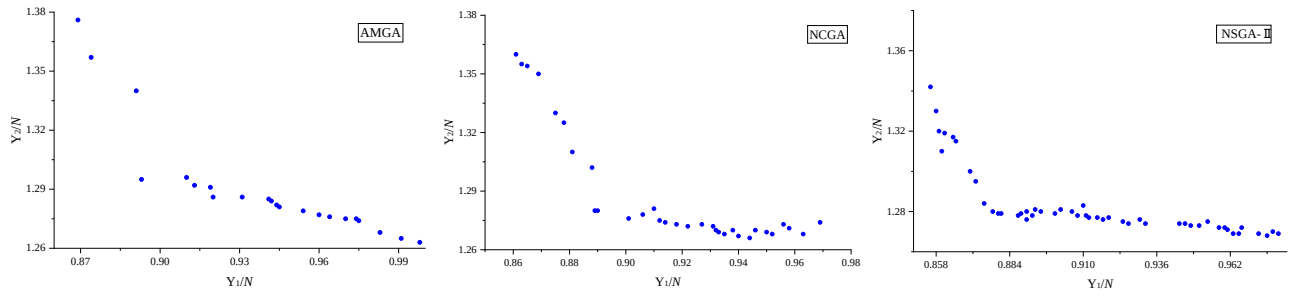

Fig. 20 Pareto solution of 3 Algorithms

The specific iterative process of the NSGA-II is shown in Figure 21. In the figure, the horizontal axis represents the number of iteration steps. The comparison between the optimal ship scheme and the initial ship scheme is shown in Table 10. The resistances of the initial ship surface case and the underwater case are 1.81 N and 2.69 N, respectively. The corresponding resistances of the optimal ship are 1.76 N and 2.55 N, respectively, and the resistance reduction rates are 2.8% and 5.2%, respectively. Among them, the friction resistance (R_f) of Case A has a small change before and after optimization, and the reduction is 1.6%. The pressure resistance (R_p) includes viscous pressure resistance (R_{pv}) and wave-making resistance (R_w). After optimization, the R_p reduction effect is obvious, and the R_p reduction rate is 4%. For Case B, the R_f reduction rate is 5.4%, and the R_p reduction rate is 5.0%. A comparison of the wave height around the initial ship and the optimized optimal of Case A is shown in Figure 22. The results show that the wave field distribution of the optimized hull is smoother, and the wave amplitude at the tail is smaller. The elevation area of the free surface of Case A near the bow is shown in Figure 23, which is called the upper wave. The bow wave amplitude of the optimized hull is reduced by about 0.0022 m. Figure 24 shows a comparison of the surface pressures of the optimal ship and the initial ship in Case B. A reduction in pressure values and the smoothness of the distribution can be seen in the figure, which results in a reduction in the radiation waves from the hull and their amplitudes. Figure 25 is a cross-section comparison diagram of the optimal ship and the initial ship.

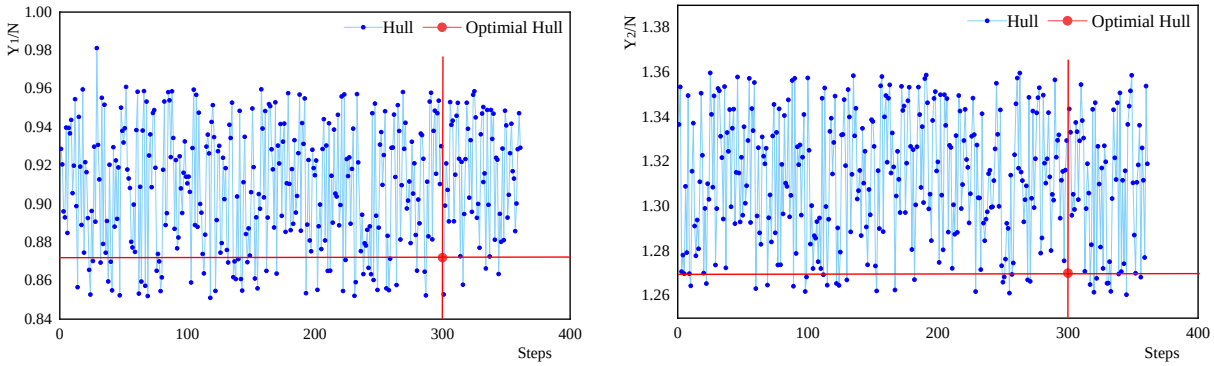

Fig. 21 Optimize iterative process

Tab. 10 Comparative analysis of optimal ship and initial ship

Ship form parameters	Initialization value	The optimal value	Design variable	The optimal value
Length (m)	1.642	1.684		
Beam (m)	0.232	0.239	w_1	0.003
Draft (m)	0.0868	0.0868	w_2	0.289
V (m/s)	1.2	1.2	w_3	0.006
C_b of Case A	0.55	0.52	w_4	0.007
∇ of Case A (m^3)	0.01826	0.01826	w_5	0.229
∇ of Case B (m^3)	0.03126	0.03126	w_6	0.232
R_t of Case A (N)	1.810	1.760	R_t reduction rate	2.8%

R_t of Case B (N)	2.690	2.550		5.2%
R_f of Case A (N)	1.230	1.210	R_f reduction rate	1.6%
R_f of Case B (N)	2.410	2.280		5.4%
R_p of Case A (N)	0.580	0.557	R_p reduction rate	4.0%
R_p of Case B (N)	0.280	0.266		5.0%

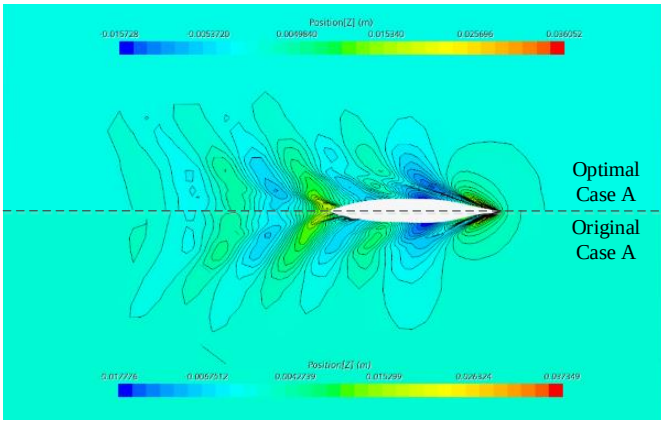

Fig. 22 Comparison of Kelvin waves between optimal ship and initial ship of case A

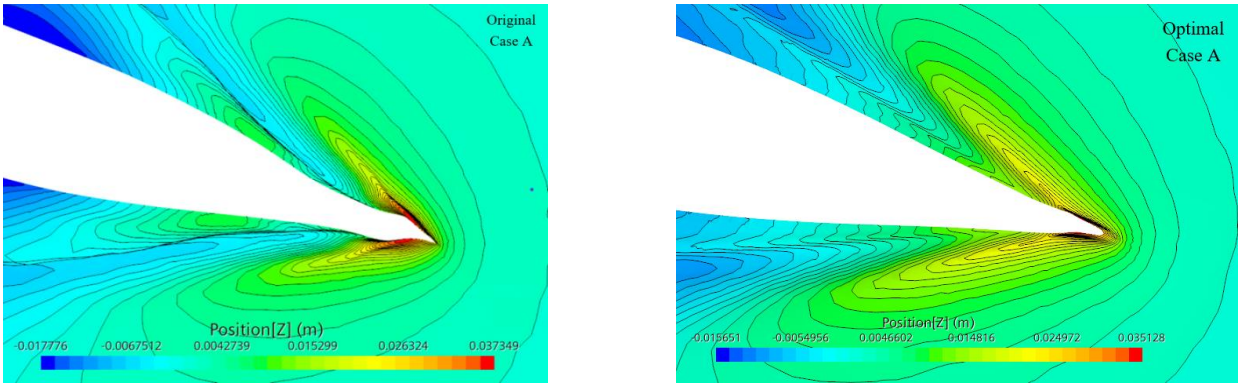

Fig. 23 Comparison of bow wave between optimal ship and initial ship of Case A

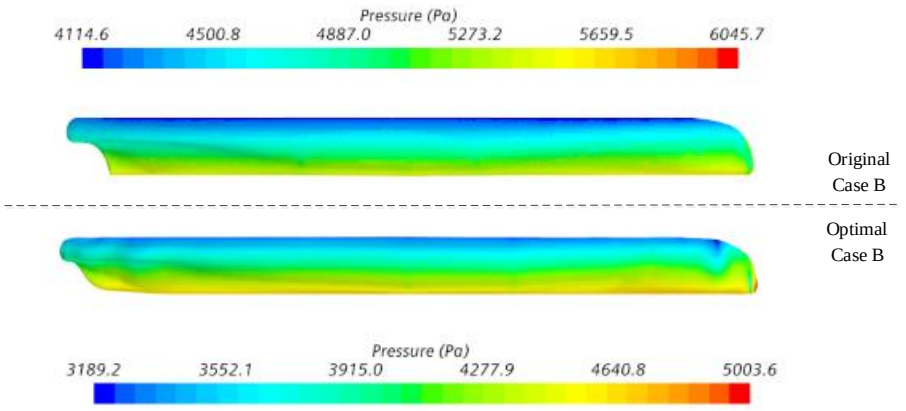

Fig. 24 Pressure distribution diagram of optimal ship and initial ship of Case B

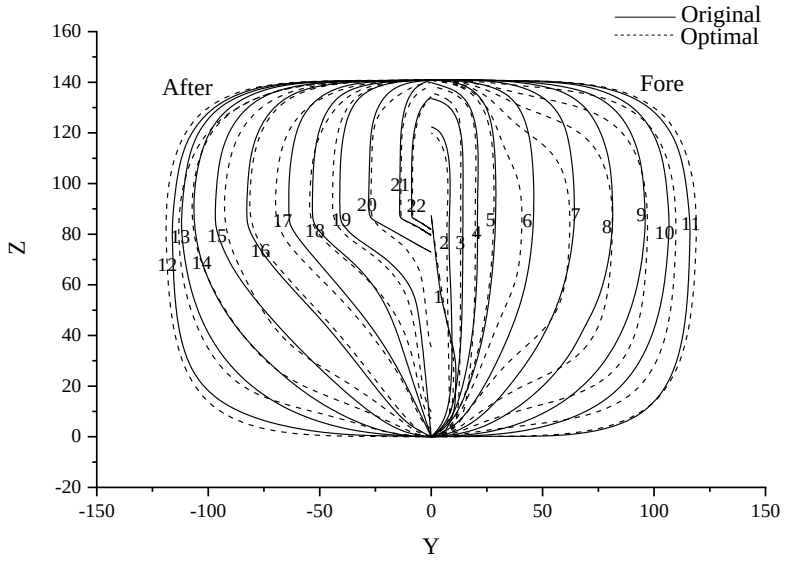

Fig. 25 The cross-section line comparison between the deterministic optimization scheme and the initial scheme

6. Uncertainty interval optimization

6.1 Interval analysis

There are three types of solutions for uncertain optimization problems: stochastic programming, fuzzy programming, and interval programming. The theory of stochastic programming is relatively mature and widely used, but it is difficult to obtain accurate probability distributions from practical problems. The research on fuzzy linear programming is also relatively mature, but fuzzy nonlinear programming requires further research. Interval programming is a relatively new field of study. Therefore, research on the uncertainty interval optimization of ship form design is conducted in this paper. Interval analysis methods do not need to know the exact probability distribution or fuzzy membership function. The methods express the variation range of uncertainty parameters through intervals. The amount of required sample information can be reduced to a certain extent. Therefore, this method is increasingly used in the optimization design of ships.

An interval is a bounded closed set of real numbers, which can be expressed as follows [30]:

$$A^I=\left[A^L,\ A^U\right]=\left\{X|A^L\le X\le A^U,\ X\in R\right\} \tag{7}$$

In the formula, the superscripts *I*, *L*, and *U* represent the interval, the lower bound of the interval, and the upper bound of the interval, respectively. The interval is a real number if and only if $A^L = A^U$.

Intervals can also be described as follows:

$$A^I=\left(A^m,\ A^w\right)=\{X|A^m\text{-}A^w\le X\le A^m+A^w\} \tag{8}$$

In the formula, *m* is the midpoint of the interval, and *w* is the radius of the interval.

When there are uncertain factors in the problem, and the interval analysis method is used to deal with it, the uncertainty interval optimization problem can be expressed as follows:

$$\begin{cases} \min F(X,R) \\ s.t.g_j(X,R)\le b_j^I=\left[b_j^L,b_j^U\right],\ j=1,2,\cdots l,\ X\in\Omega^n \\ R\in R^I=\left[R^L,R^U\right],\ R\in R_i^I=\left[R_i^L,R_i^U\right],\ i=1,2,\cdots q \end{cases} \tag{9}$$

In the formula, X is the design variable; R is the uncertain variable; and F and g are the objective function and the constraint function, respectively, which are nonlinear continuous functions about the design variable X and the uncertain variable R. R is a fluctuation interval. For any X, the values of the objective function and the constraints constitute an interval.

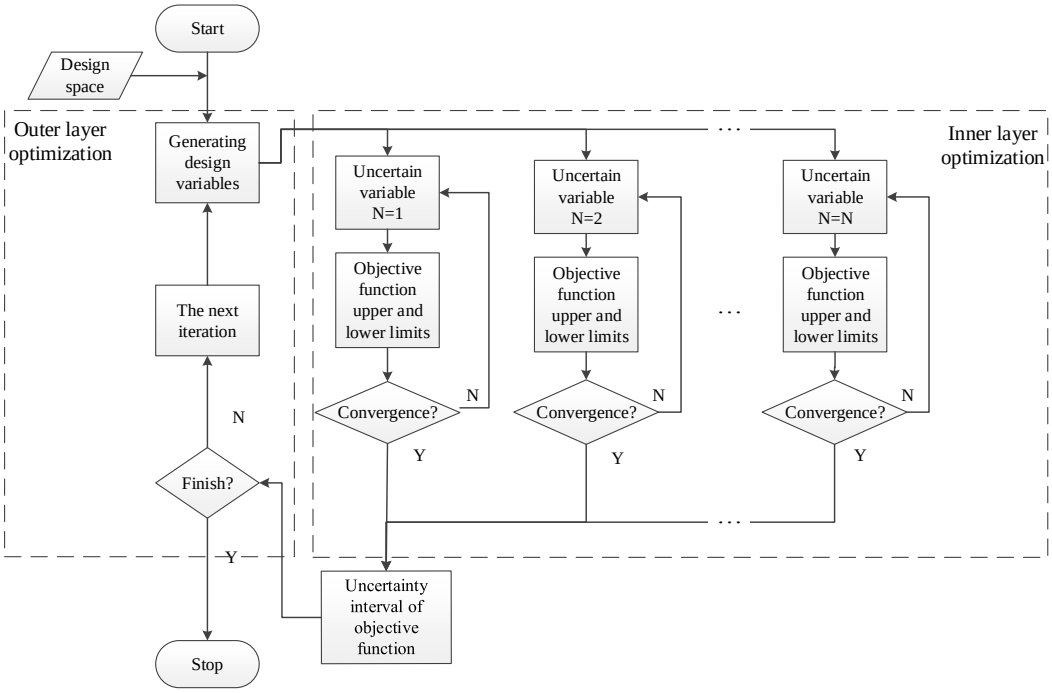

Fig. 26 Multi-interval double-layer nesting flowchart

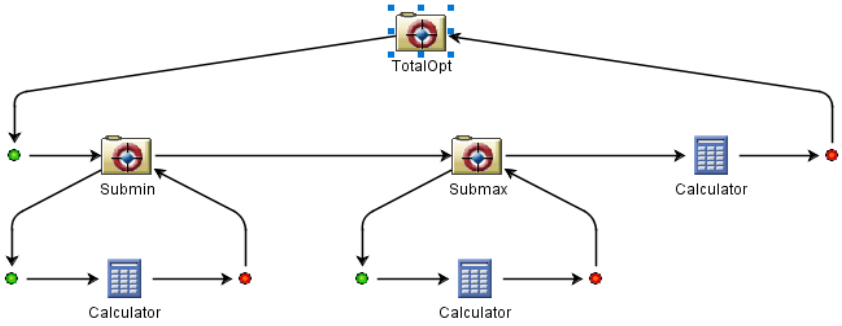

Fig. 27 Uncertainty Interval Optimization Framework

Figure 26 is a flow chart of multi-interval and two-layer nested optimization. The interval analysis method is used to embed uncertain factors into the optimization system. N uncertain factors establish N working conditions, taking one uncertainty factor as an example. The optimization algorithm and design variables are first selected in the design space and passed to the inner optimizer. In the inner optimizer, when the design variables take fixed values, the uncertain factors are represented by interval numbers. At the same time, an appropriate optimization algorithm is selected, and the upper and lower bounds of the optimization objective function in the uncertainty interval are calculated. If they converge, the uncertainty interval of the objective function is passed to the outer optimizer. The outer optimizer is mainly used for designing a variable search to find the optimal solution. If it converges, the iteration stops; if not, the loop iteration continues until convergence. Figure 27 shows the uncertainty interval optimization framework established in Isight.

In this paper, the SSS was used as the mother ship. The interval optimization analysis method was

applied to the ship form design, and the fusion factor of the six initial cross-sections was used as the design variable. The accuracy of the previously obtained response surface surrogate model is taken as the uncertainty variable. Three groups of different precisions were selected for analysis, and the value ranges were 5%, 10%, and 15% above and below the initial value. The resistance of the surface case and the underwater case was linearly weighted and integrated into the resistance value R_t for measuring the cross-domain case. The median and radius of R_t were selected as the optimization objectives, and the influence of surrogate models of different precisions on the objective function was examined.

6.2 Interval optimization design

To analyze the influence of the accuracy of the surrogate model on the objective function, the effects of surrogate models with accuracies within the [95%–105%], [90%–110%], and [85%–115%] ranges on the median and radius of the resistance of the cross-domain SSS were investigated. The double nested optimization system designed by Li et al. [31] was used to examine an uncertain robust optimization ship design. The NSGA-II, which has a strong exploration performance, a wide optimization range, and a high degree of group collaboration, was used by outer layer. The multi-island genetic algorithm (MIGA), which has better global search ability and computational efficiency, was used by inner layer.

The MIGA was selected by inner layer, and the subgroup size, the number of islands, and the genetic algebra were all set to 5. The NSGA-II was selected by outer layer, the population size was set to 40, and the genetic algebra was set to 50. A two-layer nested optimization system was used to solve the target resistance median and radius. The optimization results are shown in Table 11.

Tab. 11 Uncertainty Interval Optimization Results

Scheme	Optimization	w_1、w_2、w_3、w_4、w_5、w_6	Surrogate model accuracy	Median (Optimal solution) and Radius of R_t	Compared with NSGA-Ⅱ/%	Compared to the original plan/%
1	Original plan	-	-	Rt=2.250	+4.41	0
2	AMGA	[0.704,0.413,0.407 0.003,0.384,0.004]	1	Rt=2.168	+0.32	-3.64
3	NCGA	[0.607,0.312,0.006, 0,0.342,0.008]	1	Rt=2.166	+0.23	-3.73
4	NSGA-Ⅱ	[0.003,0.289,0.006, 0.007,0.229,0.232]	1	Rt=2.161	0	-3.96
5	Interval optimization	[0.823,0.368,0.181, 0.038,0.062,0.175]	[95%-105%]	m=2.1088 w=0.0747	-2.42	-6.28
6	Interval optimization	[0.021,0.063,0.743, 0.960,0.024,0.644]	[90%-110%]	m=2.2039 w=0.0426	+1.93	-2.05

7	Interval optimization	[0.926,0.313,0.786, 0.089,0.725,0.202]	[85%-115%]	m=2.1861 w=0.0562	+1.16	-2.84

Table 5 shows the optimization results for the accuracy of the surrogate model with a single uncertainty factor. The results in Table 5 show that compared with NSGA-II deterministic optimization, the surrogate model with an accuracy of 95% reduces the objective function value by 2.42%. Surrogate models with accuracies within the [90%–110%] and [85%–115%] ranges increase the objective function by 1.93% and 1.16%, respectively. Among the chosen uncertainties, the change in the accuracy of the surrogate model with accuracy within the [95%–105%] range has a positive effect on the objective function. Surrogate models with accuracies within the [90%–110%] and [85%–115%] ranges have a negative impact on the objective function. Scheme 4 is the only one among the three groups of interval optimization schemes that reduces the value of the objective function, but its R_t radius is, at most, 0.0747. This shows that the accuracy of the surrogate model is the weakest robustness to the objective function when the accuracy of the surrogate model varies within the [95%–115%] range.

The median R_t of the optimization results obtained by schemes 4, 5, and 6 is around 2.1. However, the R_t radius of the surrogate model with an accuracy of [90%–110%] is only 0.0426, and the fluctuation range is small. This shows that the surrogate model within the accuracy range is more robust to R_t. It can be seen from Scheme 6 that the surrogate model with an accuracy of [85%–115%] has little effect on R_t and increases by only 1.16% compared to NSGA-II deterministic optimization. However, the R_t radius, 0.0562, is relatively large. This shows that its robustness to the objective function is weak, but it is still better than the value of the mother ship. Therefore, the interval analysis method can be introduced into uncertain optimization to weaken the influence of uncertain factors on the objective function and to ensure the actual operability of the scheme.

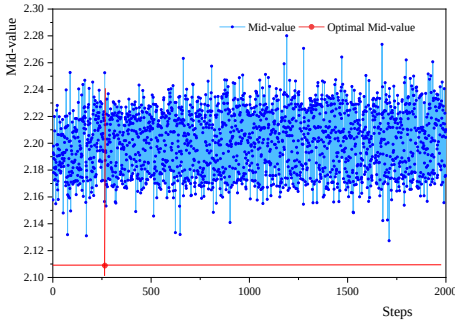

(a) [95%-105%] accuracy

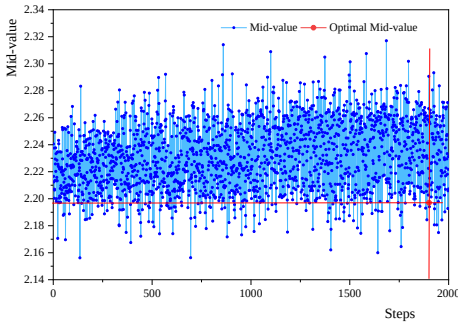

(b) [90%-110%] accuracy

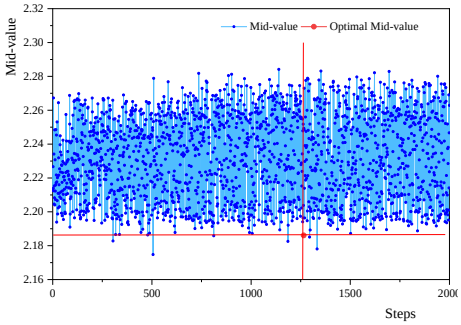

(c) [85%-115%] accuracy

Fig. 28 Uncertainty Interval Optimization Framework

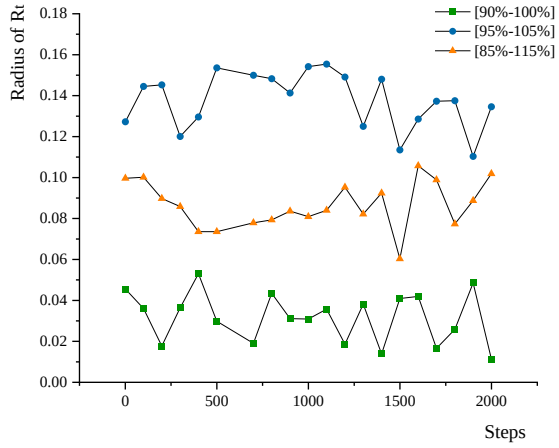

Fig. 29 R_t radius fitting diagram

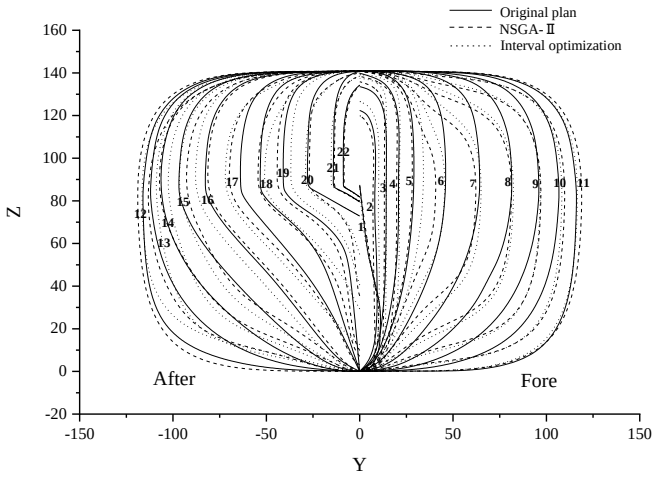

Fig. 30 Cross-section comparison diagram

Figure 28 shows that under this optimization algorithm, the objective functions of the three precision surrogate models have a good convergence trend, and the results fluctuate around 2.1. The change in the radius of the objective function in Figure 29 shows that the R_t of the surrogate model with an accuracy of [90%–110%] increased after uncertainty analysis is added. However, the radius value of the objective function is small, indicating that its robustness is high. On one hand, this proves that the robust optimal solution obtained with the interval analysis method is feasible in the uncertainty quantification process. On the other hand, it can also be seen that after the influence of uncertainty is considered, the value of the objective function increases slightly. However, its stability is better, which is more conducive to ensuring the low failure rate of the scheme. Therefore, the results obtained with the surrogate model with an accuracy of [90%–110%] are used as the best solution for interval optimization. The cross-sectional views of the initial scheme, the deterministic optimization scheme, and the uncertain optimization scheme are shown in Figure 30. The initial hull shape is represented by a solid line, the optimal hull shape under the determined optimization is represented by a dashed line, and the optimal ship shape for interval optimization is represented by a dotted line. This figure shows that there is little difference between the deterministically optimized ship and the uncertainly optimized ship. Compared with the initial ship, the form of the middle of the hull of the deterministically optimized ship scheme and the uncertain optimized scheme is slightly plumper than that of the initial scheme. The bow and stern areas are thinner than those of the original ship. The influence of the bow wave on the resistance of the SSS is changed. The distribution of the flow field at the tail is improved to achieve the effect of resistance reduction.

7. Conclusion

This paper is based on the connections between the three basic disciplines. A multi-objective optimization process was established, and the ship form optimization problem of the SSS for cross-domain “surface-underwater” sailing was defined. Resistance of the SSS in the surface case and the underwater case with a diving depth of 0.48 m were the two goals of this study. The aims were to reduce resistance and optimize the overall form of the SSS. Therefore, two main goals were pursued. First, an efficient and practical automated computing platform was established. Second, the optimal ship form scheme with the least resistance under cross-domain sailing was found. Finally, based on the deterministic optimization above, the interval analysis method was introduced to investigate robust ship design optimization.

(1) A self-fusion method based on modifying the shape of the cross-section was adopted for the optimization process. The modified ship surface is smooth enough to be used for subsequent studies.

(2) The accuracy and efficiency of three multi-objective optimization algorithms, NSGA-II, NCGA, and AMGA, were compared and analyzed. It was found that the NSGA-Ⅱ was the most suitable for this study. The optimization results show that compared with the initial ship, the cross-domain resistance of the optimized ship was reduced by 2.8% and 5.2%. The shape of the shoulders of the hull became more slender, and the shape of the hull in the middle became relatively full. For the surface case, the shape lines of the bow and stern areas of the hull were thinner than those of the initial ship. The influence of bow waves on the SSS was changed, and the distribution of the stern flow field was improved. The optimized bow wave amplitude was reduced by about 0.0022 m. In the underwater case, the pressure in the high- and low-pressure areas of the optimized ship was reduced by 1042 Pa and 925 Pa, respectively, compared with the initial ship. The radiation wave and its amplitude from the hull were reduced.

(3) There are many uncertain factors in ship optimization design. This can lead to deviations in the optimization scheme. Therefore, it is of great significance to apply uncertain optimization to ship scheme design. The effect of surrogate models of different precisions on the objective function was investigated. The change in the accuracy of an approximate model with [95%–105%] accuracy had a positive effect on the objective function. The surrogate models with [90%–110%] and [85%–115%] accuracy had a negative impact on the objective function. Among them, the R_t of the surrogate model with an accuracy of [90%–110%] after adding the uncertainty analysis increased but still outperformed that of the initial ship. The minimum radius value of its objective function floated around 0.02, indicating its high robustness. It was demonstrated that a robust optimization solution obtained by using the interval analysis method in the uncertainty quantification process is feasible.

Further work can be carried out from the following perspectives:

(1) A surrogate model established through small sample learning could reduce the time cost and could introduce complex marine environmental elements, such as waves and ice loads, for more in-depth research.

(2) The effects of multiple uncertain variables on the objective function could be investigated. For example, the constraint that the molded volume of displacement is constant in this study could be transformed into a variable interval, and the influence on the objective function under the coupling effect of the molded volume of displacement and the surrogate model accuracy could be considered.

(3) Uncertainty analysis methods can be changed to utilize Six Sigma levels for reliability analysis and optimization.

Acknowledgement

This work is supported by the National Natural Science Foundation of China (Grant No. 51879023).

Reference

[1]. ZHOU Hongguang, MA Aimin, XIA Lang. A Research on the Development of the Unmanned Surface Vehicles[J]. National Defense Science & Technology, 2009, 30(6): 17-21.

[2]. LI Bing, GUAN Guan, GUAN Guizhu, QI Zhentao, LIN Yan. Design Optimization of Special Semi-Submersible Unmanned Vehicle[J]. Ship Engineering,2018,40(06):95-99+105.

[3]. Alleman P, Kleiner A, Steed C. Development of a new unmanned semi-submersible (USS) [R]. OMB No.0704-0188, Washington:

National Maritime Intelligence Office, 2012.

[4]. HUO Cong, DONG Wencai. Free Running Tests on Navigation Mode Conversion of a Latent High Speed Craft[J]. Journal of Shanghai Jiao Tong University, 2016,50(08):1180-1185.

[5]. HARRIES S. ABT C. and HOCHKIRCH K. Modeling meets simulation-process integration to improve design[C]. Honorary Colloquium for Prof. Hagen, Prof. Schluter and Prof. Thiel. Duisburg, Germany: University of Duisburg-Essen, 2004.

[6]. Choi, H.J., Chun, H.H. and Jeong, S.H., 2005. Fundamental Study for the Development of an Optimum Hull Form. Journal of Ocean Engineering and Technology, 18(3), pp.32-39.

[7]. Choi, H.J., Seo, K.C., Kim, B.E. and Chun, H.H., 2003. Development of an optimum hull form for a container ship with minimum wave resistance. Journal of the Society of Naval Architects of Korea, 40(4), pp.8-15.

[8]. Kim, W.J. and Van, S.H., 2000. Comparisons of turbulent flows around two modern VLCC hull forms. Proceedings workshop on Numerical Ship Hydrodynamics: Gothenburg 2000, Gothenburg, Sweden, 8-10 December 2010.

[9]. Liu Q , Feng B , Liu Z , et al. The improvement of a variance-based sensitivity analysis method and its application to a ship form optimization model[J]. Journal of marine science and technology, 2017, 22(4):694-709.

[10]. KIM Hyunyu1 Y., YANG Chi. A new surface modification approach for CFD-based hull form optimization[J]. Journal of Hydrodynamics, 2010, 22(5Suppl.): 520-525.

[11]. Softley, J. and Schiller, T.R., 2002. An approach to advanced ship design using parametric design templates. Transactions - Society of Naval Architects and Marine Engineers, 110, pp.245-258.

[12]. Harries, S., Abt, C. and Heimann, J., 2003. From redesign to optimal hull line by means of parametric modeling. 2nd International Conference on Computer Applications and Information Technology in the Maritime Industries (COMPIT 2003), Hamburg, Germany, May 2003.

[13]. Lowe, T.W. and Steel, J., 2003. Conceptual hull design using a genetic algorithm. Journal of Ship Research, 47, pp.222-236.

[14]. Jacpuin, E., Derbanne, Q., bellèvre, D., Cordier, S. and Alessandrini, B., 2004. Hull form optimization using a free surface RANSE solver. 25thSymposium on Naval Hydrodynamics. Newfoundland, Canada, 8-13 August 2004.

[15]. Peri D, Campana E F. High-fidelity models and multi-objective global optimization algorithms in simulation-based design[J]. Journal of Ship Research, 2005, 49(3):159-175.

[16]. QIAN J K, MAO S F, WANG X Y, et al. Ship hull automated optimization of minimum resistance via CFD and RSM technique[J]. Journal of Ship Mechanics,2012, 16(1/2): 36-43 (in Chinese).

[17]. Bogumil Kaminski. A method for the updating of stochastic Kriging meta-models[J]. European Journal of Operational Research, 2015, 247(3): 859-866.

[18]. Li N, Chen M, etc. Optimization research of ship parameters for FRP fishing vessels based on GRNN and genetic algorithm[J]. Ship Engineering, 2012, 34(4): 18-22.

[19]. Tomasz Praczyk. Using evolutionary neural networks to predict spatial orientation of a ship[J]. Neuro-computing, 2015, 166(10): 229-243.

[20]. Cen M, Cheng R W. Optimal design of system reliability using interval programming and genetic algorithms[J]. Computers and Industrial Engineering, 1996, 31(1-2):237-240.

[21]. Cen M, Cheng R W. Optimal design of system reliability using interval programming and genetic algorithms[J]. Computers and

Industrial Engineering, 1996, 31(1-2):237-240.

[22]. Li F Y, Li G Y, Zheng G. Uncertain multi-objective optimization method based on interval[J]. Chinese Journal of Solid Mechanics, 2010, 31(1): 86-93.

[23]. Gong G W, Sun J. Theory and application of interval multi-objective evolutionary optimization[M]. Beijing: Science Press, 2013. 1-22.

[24]. Ktem H, Erzurumlu T, Kurtaran H. Application of response surface methodology in the optimization of cutting conditions for surface roughness[J]. Journal of Materials Processing Tech, 2005, 170(1-2):11-16.

[25]. Hirayama, T., Takayama, T., Hirakawa, Y., Koyama, H., Kondo, S., Akiyama, M.,2005. Trial experiment on the submersible surface ship utilizing downward lift. In: Conference Proceedings of the Japan Society of Naval Architects and Ocean Engineers, vol. 1, pp. 233–234.

[26]. Ueno M. Hydrodynamic derivatives and motion response of a submersible surface ship in unbounded water[J]. Ocean Engineering, 2010, 37(10):879-890.

[27]. Song Kewei, Guo Chunyu, Sun Cong, Li Ping. Research on the full-scale ship resistance simulation and the scale effect[J]. Journal of Huazhong University of Science and Technology (Nature Science Edition), 2021,49(06):74-80.

[28]. Hong Zhichao. Prediction and Optimization of Ship Hydrodynamic Using CFD Technology [D].Dalian University of Technology, 2018.

[29]. Junfang L I, Zhang B. Probabilistic Load Flow Based on Improved Latin Hypercube Sampling With Evolutionary Algorithm[J]. Proceedings of the CSEE, 2011, 31(25):90-96.

[30]. Gong Dunwei, Sun Jing. Interval Multi-objective Evolutionary Optimization Theory and Application [M]. Science Press, 2013.

[31]. Li Dongqin, Dai Jingjing, Li Guoguan, Zhang Yili, Li Peng. Ship Uncertainty Robust Design Optimization Based on Interval Analysis Method[J]. Ship Engineering, 2018, 40 (7).